Light particle emission near 0° in the reaction $^{20}Ne+^{181}Ta$ at $E/A=85$ MeV

D. A. Roberts, F. D. Becchetti, J. A. Brown, and J. W. Jänecke
Physics Department, University of Michigan, Ann Arbor, Michigan 48109

D. Shen and Z. W. Yin
Shanghai Institute of Ceramics, Academia Sinica, Shanghai 200050, China

A. Nadasen
Department of Natural Sciences, University of Michigan–Dearborn, Dearborn, Michigan 48128
(Received 8 July 1991)

Energetic light ions (primarily protons and alphas) were detected in heavy-ions collisions of ^{20}Ne with ^{181}Ta at an energy $E/A=85$ MeV. Analysis of the spectral shapes and angular distributions using a standard moving-source model requires that the source velocity approaches the beam velocity at zero degrees. Apparent source temperatures are only modestly increased at this energy compared to apparent source temperatures in reactions at energies $E/A=9$ to 40 MeV, indicating a possible saturation effect in the projectile nucleus. The production of very energetic light ions (where the light-ion energy approaches the total beam energy) was not seen in this experiment, possibly indicating that a previously proposed massive cluster transfer mechanism is invalid, or suppressed at this higher energy.

PACS number(s): 25.70.−z, 25.70.Mn, 24.10.−i

I. INTRODUCTION

Projectile fragmentation, with Fermi motion of the nucleons within the projectile, is often suggested as the primary mechanism for the production of energetic light ions with velocities greater than that of the beam [1–3] in heavy-ion collisions. With this model the fragmentation may be modeled as being derived from a source moving with a source velocity (v_s) characterized by an apparent temperature (T_s) with a Maxwellian velocity distribution. Such a model will be described later in this paper and the data will be interpreted on the basis of this model.

At low bombarding beam energies, the production of light ions is dominated by compound-nucleus (CN) evaporation. The peak in production cross section is below the beam energy, measured in MeV/nucleon, and has an energy spectrum characterized by a temperature (T_{CN}) of a few MeV. The low-energy portion of the energy spectrum is cut off by the projectile–compound-nucleus Coulomb barrier. The high-energy portion of the energy spectrum is believed to be due to preequilibrium emission, where the apparent emission temperature is greater than the compound-nucleus temperature. Thus, when we speak of temperatures in this context, it is not implied that thermal equilibrium has been achieved with the nucleus, and these temperatures do not necessarily correspond to typical nuclear temperatures.

The energy end points of the light-particle spectra are determined by either three-body limits (projectile breakup) or projectile breakup followed by direct transfer reactions, which results in a two-body limit [14–16]. Since the grazing angles for these reactions are still quite large, quasielastic processes can be significant near the grazing angle, with deep-inelastic processes dominating the spectra for angles greater than the grazing angle. Thus, the particle emission spectra are essentially thermal, except near the grazing angle where they appear nonthermal.

At higher beam energies the light-ion production spectra are dominated by the breakup of the projectile [15]. Production cross sections peak at the same energy, measured in MeV/nucleon, as the beam energy and are approximately Gaussian in momentum space about this peak. The spectral slope parameter near this peak is still low, roughly equal to the Fermi temperature of a few MeV, and is essentially unaffected by increased beam energy. The high-energy tails of these spectra exhibit spectral slope parameters that are larger than slope parameters measured near the breakup maximum. The energy end points of these spectrum can approach the full beam energy, implying a collective coherent mechanism. The question then remains as to whether this coherent mechanism, survives at higher bombarding energies. An example of such a coherent mechanism is massive cluster transfer [16,17].

Measurement of γ rays can also yield important information about heavy-ion collision mechanisms. Particularly, the angular distribution of the γ rays can be used to determine the γ-ray source velocity [18,19]. Assuming that the source of the γ ray is nucleon-nucleon bremsstrahlung, then the velocity of the source should be the nucleon-nucleon velocity, e.g., about half the beam velocity. If, on the other hand, the source of the γ rays is a deep-inelastic collision, then the velocity of the source should be the nucleus-nucleus velocity [18]. In either case, the slope of the angular distribution is determined by the velocity of the source, assuming isotropic emission of the γ rays in the frame moving at the source velocity. Study of correlations between γ rays and charged particles in heavy-ion collisions can also provide information about the apparent temperature of the collision system.

Two-particle correlation studies are also important tools in the understanding of heavy-ion collisions. Such correlations can lead to information about nuclear sources such as temperature [20], nuclear equation of state [21], source sizes [22], and nuclear cross sections in the nuclear media [21]. In recent years, such two-particle correlation data have begun to appear [22–31]. These studies include both correlations between two charged particles, e.g., two-proton correlations, and between a neutron and a charged particle, e.g., a neutron and an alpha particle. The information in these studies appears to be in the low-momentum-transfer portion of the transfer function. The point of interest for the subject of this paper is that the temperature measured in such correlation studies are often much lower, by factors of 2 or more, than the slope temperature of singles spectra measured in the same experiments. It has been suggested that the lower temperatures measured in these studies can be either manifestations of quantum statistics [22] or the possibility that Boltzmann factors do not adequately describe excited-state populations within the nuclear media [32], e.g., due to the presence of nuclear isomeric levels.

In a previous paper [14] we presented results from heavy-ion collisions in the energy range $9 \leq E/A \leq 40$ MeV and reported light-ion production at, and near, 0°, specifically alpha particles with spectra end-point energies which, in some cases, approach the full beam energy. This paper will report on a similar experiment at an energy per nucleon of 85 MeV. The analysis of the data from the previous experiments indicated spectral slope parameters and source temperatures roughly twice as large as those reported for complex fragment emission [20,33–39]. This paper, in contrast, will report source temperatures closer to the temperatures reported for the complex fragment production, with spectra end-point energies well below the beam energy indicating a reduction in emission of single light ions with high energies and a corresponding increase in the multiplicity of emitted light ions.

II. EXPERIMENT

The experiment was performed at the Michigan State University National Superconducting Cyclotron Laboratory (MSU-NSCL) in East Lansing, Michigan, with the $K1200$ cyclotron in the 92-in. scattering chamber. The beam intensities were 1 particle nA, or less, and were necessarily low to keep detector dead time, and particle pile up, to acceptable limits—less than a few percent.

A. Detectors

In this experiment we have used a stopped beam technique, as previously described [14], to measure light-ion and projectile-like fragment (PLF) production at, and near, 0°. The stopped beam technique was used to avoid the direct beam, and the small angle heavy-ion-target scattering associated with this type of experiment, thus permitting the measurements to be continued to 0°. We used an array of high stopping power BGO glass scintillators [40–42]. The use of BGO scintillators avoids the use of magnetic spectrometers usually used for such measurements [16,17].[1]

We have employed a set of three particle telescopes to obtain angular distributions from 0° to 90°. Each particle telescope consisted of a 2.0-mm-thick × 50.8-mm-diam Si(Li) solid-state detector backed by a 254-mm-thick × 50.8-mm-diam BGO crystal attached to an Amperex XP2252 fast photomultiplier tube. The stopping power of the BGO was adequate to stop a 3-GeV alpha particle. These detectors formed a ΔE-E telescope, with the solid-state detector forming the ΔE signal, and the BGO detector forming the stopping E signal. The efficiency of the detector above 200 meV/nucleon is less than unity due to nuclear reactions within the scintillator, but could be estimated from other data [14]. The BGO detector at 0° had a 9.5-mm-diam collimator in front of the solid-state detector; this collimator allowed us to obtain data from the other detectors at large angles without excessive dead time caused by the 0° telescope. The detectors were typically situated at 70–100 cm behind a stopping tantalum target. The tantalum target was of adequate thickness to just stop the impinging beam and was connected to a current digitizer system to measure the beam current.

In addition, a smaller BGO detector 150 mm long × 40 mm diameter was placed at −15°, and a NaI (Tl) detector 100 mm × 100 mm diameter was placed at −90°. These two additional monitors were used as beam monitors, as a cross check of the integrated beam current.

Particle identification (PID) spectra are shown in Figs. 1 and 2. In these figures the vertical axis is pulse height from the solid-state detector (ΔE), and the horizontal axis is light output from the phototube attached to the

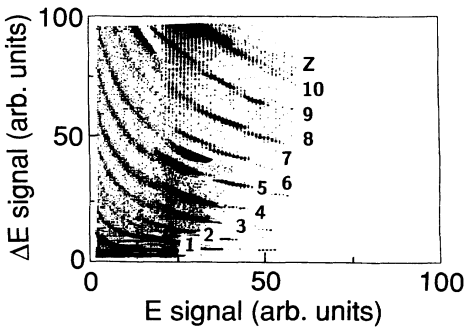

FIG. 1. This figure shows a particle identification spectrum which is the summation of several calibration runs. The vertical axis is the linear signal from the solid-state detector, the front element in the particle telescope. The horizontal axis is the light output from the last dynode of the photomultiplier which was attached to a BGO crystal, the last element in the particle telescope. This spectrum was taken with the amplifier from the solid-state detector set at a low gain; note that bands from $Z = 1$ (H) to $Z = 10$ (Ne) are visible.

[1]The BGO crystals were supplied as part of a National Science Foundation funded US-China cooperative science research project with Shanghai Institute of Ceramics, Peoples Republic of China.

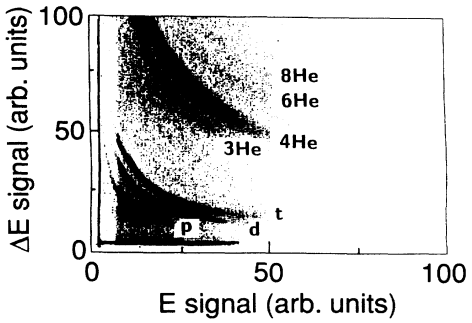

FIG. 2. This particle identification spectrum was taken with the amplifier from the solid-state detector set to a high-gain value and was used to identify the low-Z fragments. Note that all three isotopes of hydrogen are easily distinguished, p,d,t, and that three isotopes of helium are also clearly discernable (^{3}He,^{4}He,^{6}He). Evidence also exists in these spectra for the isotope ^{8}He.

BGO crystal (E-ΔE). The light output was taken from a dynode in the phototube, and the anode was run in a semisaturated mode. We were then able to obtain a good timing signal [40] from the anode, with a fast rise time, and a linear signal from the dynode, with a slower rise time.

A particle identification spectrum is shown in Fig. 1. This particle identification spectrum was taken with the amplifier from the solid-state detector set at a low gain. Note that bands from $Z=1$ (H) to $Z=10$ (Ne) are visible; this figure is the summation of several calibration runs as described below. This gain setting was used to identify PLF, where PLF is defined as $2<Z_{\rm PLF}\leq Z_{\rm beam}$.

A second particle identification spectrum is shown in Fig. 2. This particle identification spectrum was taken with the amplifier from the solid-state detector set to a high gain value and was used to identify the low-Z fragments. Note that all three isotopes of hydrogen are easily distinguished p,d,t and that three isotopes of helium are clearly discernible (^{3}He,^{4}He,^{6}He). Evidence also exists in these spectra for the isotope (^{8}He), statistics are too low to allow useful spectral parameters to be extracted for this isotope.

The pulse heights from the solid-state detectors and the scintillators were digitized via CAMAC analog-to-digital converter (ADC) and charge-to-digital converter (QDC) modules, respectively. Particle identification via pulse-shape discrimination (PSD) could not be accomplished in the BGO detectors due to the poor signal-to-noise ratio [40] associated with the low light output of the BGO crystals. Pileup events were eliminated by keeping the beam currents low and via hardware pileup gates. Particle types were identified by offline software gating on the two-dimensional PID spectra.

Energy calibration of the particle telescope was done with a separate beam fragmentation experiment, cosmic-ray muon calibrations, and the use of (^{22}Na) γ-ray sources. The beam fragmentation experiment consisted of placing a stopping Ta target upstream of the scattering chamber, before the last analyzing magnet. The analyzing magnet was then set to a known ion momentum, and the fragmentation products produced were sent, after bending by the last magnet, directly into individual detectors located at $\Theta=0°$. As a result, each of the isotopes of interest ($p,d,t,^3$He,^{4}He,^{6}He) was selected with a well-defined energy centroid (although not a well-defined width). Table I shows the energies of the various isotopes produced in this fragmentation experiment. Cosmic-ray muons were also used as a means of calibrating the energy response of the BGO crystals [43,44]. The cosmic rays, being mostly minimum ionizing muons, have a well-defined peak in a light-output spectrum from the BGO crystals. The peak in the cosmic-ray light-output spectrum has a well-defined γ-ray equivalent. γ rays from (^{22}Na) then allowed us to calibrate the low-energy portion of the BGO light-output spectrum, and were used to check for gain drifts in the tubes during the course of the experiment. Any gain drifts were stabilized to less than 5% during the experiment, or by software correction during offline replay of the event tapes.

There are three major sources of error in the calibration of the detectors. First, the data from the fragmentation experiment were fit, by a least-squares method, to polynomials of third order. The uncertainties in the parameters derived from this fit lead to a maximum uncertainty of the calculated energy of any $Z=1$ or 2 isotope of not more than 8%. Second, the intrinsic resolution of the BGO scintillators is not better than 5–10%, depending on the energy [40,41]. Last, nuclear reactions can occur within the BGO crystal, which lowers the efficiency of the detector. This nuclear reaction effect produces low-energy tails on monoenergetic peaks. This experiment measures the continuum of fragmentation reactions, and not transitions to discrete states; thus, this nuclear reaction effect does not radically alter the shape of the spectra nor the slope parameter derived from these spectra. These effects have been estimated [43,44], and the maximum errors in each have been added in quadra-

TABLE I. Energies of fragmentation products used to calibrate detectors.

p (MeV)	d (MeV)	t (MeV)	^{3}He (MeV)	^{4}He (MeV)	^{6}He (MeV)
200	100	67	267	200	133
340	170	113	453	340	227
500	250	167	667[a]	500	333
694	347	231	925[a]	694	462
1000[a]	500	333	1333[a]	1000[a]	667[a]

[a]Fragmentation products not observed, or observed, in a lower charge state.

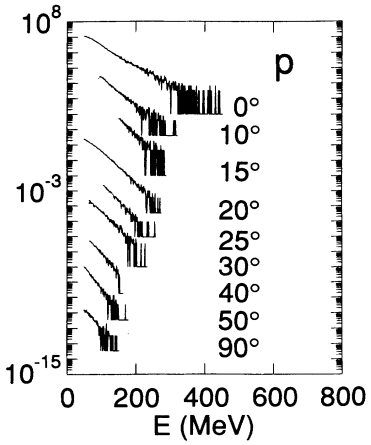

FIG. 3. The fragmentation cross sections over the range of angles for which protons were identified. It was assumed that the target thickness was equal to the incident beam range. The scaling of the cross sections on this figure is as follows: the top curve in is multiplied by a factor of 10^6, each successive curve is then multiplied by a factor which is 10^2 lower than the multiplicative factor of the curve before it. Thus, the second curve is multiplied by a factor of 10^4. The laboratory angle at which each curve was measured is indicated to the right of each curve.

ture in estimating the errors for spectral temperature parameters, both the laboratory temperature, T_{lab}, and the apparent moving source temperatures, T_s.

B. Spectra

In our previous paper we have shown [14] that the high-energy portion of light-ion (LI) spectra produced in a thick stopping target are primarily generated from the high-energy portion of the incident beam, and that the desired moving source parameters, T_s and v_s, can thus be inferred from stopping target spectra. However, unlike thin targets, the peak in the LI energy spectrum from a thick target will not be centered at $(E/A)_{\text{LI}}=(E/A)_{\text{beam}}$. The shape of such a spectrum can be calculated as an integral over the range of the incident beam in the target, as indicated below.

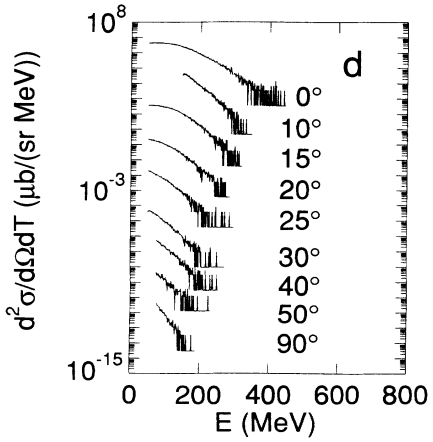

FIG. 4. The fragmentation cross sections for deuterons. The same conditions as in Fig. 3 apply.

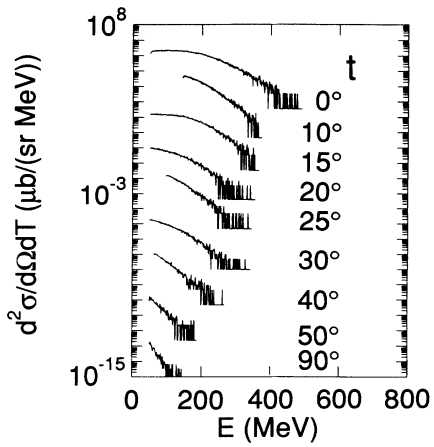

FIG. 5. The fragmentation cross sections for tritons. The same condition as in Fig. 3 apply.

Displayed in Figs. 3–8 are the cross sections over the range of angles for which each particle type was identified. The scaling of the cross sections on these figures is as follows: the top curve in each figure is multiplied by a factor of 10^6, each successive curve is then multiplied by a factor which is 10^2 lower than multiplicative factor of the curve before it; thus the second curve is multiplied by a factor of 10^4 and so on. The angle at which each curve was measured in indicated to the right of each curve.

The primary goal of the experiment was to measure the slope parameters and end-point energies of the high-energy tails in the energy spectra. It was necessary for some angles, particularly at 10°, to take high-energy and low-energy data in separate runs to avoid rate problems. For these runs only the high-energy portion of the data, above the hardware discriminators levels, is shown. The spectral slope parameters were extracted separately for each portion of the spectra.

At 0° the peak for the thick target spectra occur at $(E/A)_{\text{LI}}\sim 0.6(E/A)_{\text{beam}}$ for each LI particle type, unlike a thin target spectrum which would have

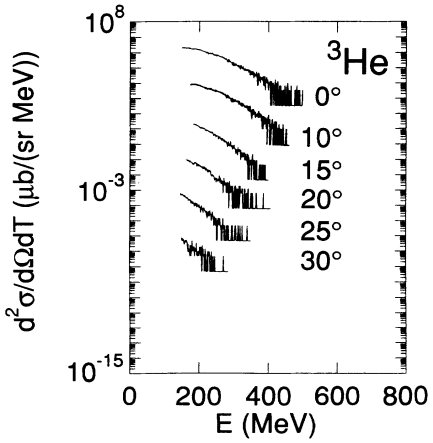

FIG. 6. The fragmentation cross sections for ^{3}He. The same conditions as in Fig. 3 apply.

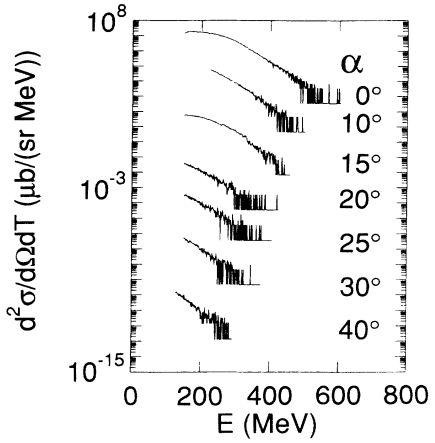

FIG. 7. The fragmentation cross sections for α. The same conditions as in Fig. 3 apply.

$(E/A)_{\rm LI} \sim (E/A)_{\rm beam}$ [14,40]. The spectra then fall off like $\sim \exp^{-E_{\rm lab}/T_{\rm lab}}$, where $E_{\rm lab}$ is the LI fragments laboratory energy, and $T_{\rm lab}$ is the spectral slope parameter—often called the laboratory temperature. At 0° the highest energy observed in the spectrum, called $E^0_{\rm max}$, can be no greater than the end-point energy of a reaction channel, that is, the kinematic limit of the reaction minus the Q value of the reaction channel.

The kinematics are typical of a many-body reaction, with a minimum of three bodies needed to keep the reaction on the mass shell. Subsequently, there are a set of phase spaces associated with each reaction—three-body phase space, four-body phase space, etc. These phase-space volumes grow ever larger with increasing incident beam energy, with the kinematic phase-space distributions largest at small momentum. Thus, as the incident beam momentum increases, the high-energy portion of an n-body channel comes into competition with the low-momentum portion of an $(n+1)$-body channel. The net result may be a decrease in the magnitude of the high-energy portion of the spectrum, thus leading to a decrease in the laboratory slope parameter and a coincident decrease in the extracted source temperature. The evidence of such a mechansim at work would be either a leveling off of apparent source temperature or even a decrease of the source temperature, with a concurrent increase in the average particle multiplicity in a collision event [45]. This mechanism is the only competition between coupled channels in the projectile breakup. As will be shown below, the laboratory slope parameters, extracted source temperatures, and particle-hit multiplicites are in agreement with this qualitative model.

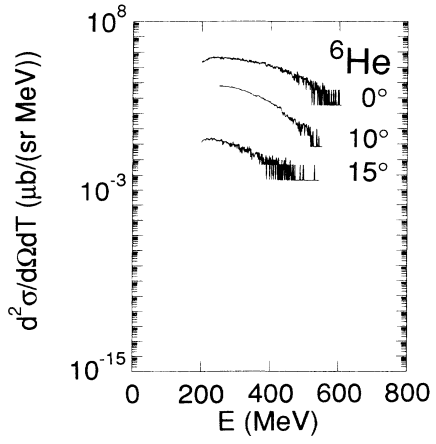

FIG. 8. The fragmentation cross sections for ^{6}He. The same conditions as in Fig. 3 apply.

The 0° spectra for alpha particles only extend to about one-third of the total beam energy in this experiment, in contrast to the previous experiments [14,16,17] at lower beam energies, where the alpha-particle energy spectra often extend to nearly the total beam energy for projectiles with $A \leq 32$. Protons, deuterons, tritons, and ^{3}He particle energy spectra extend to increasing energy in that order. The ^{6}He particle energy spectra extend to energies nearly equal to the alpha-particle spectra, although with much lower statistics. However, when measured in energy per nucleon, i.e., velocity, the proton energy spectra extended to the highest value, followed by deuterons, tritons, and ^{3}He which are nearly equal, followed by alphas and finally ^{6}He. Thus, the end point of the particle energy spectra, measured in energy per nucleon, appears to be roughly inversely proportional to the mass of the particle.

Examples of the moving-source model fits, which will be described below, are shown in Figs. 9 and 10 for proton and alpha particles, respectively, at 0°. The dotted line in these figures is the intermediate-rapidity source contribution; the dot-dashed line is the high-rapidity contribution, which may be interpreted as the projectile fragmentation contribution. These two curves are divided by a factor of 10 for clarity. The solid double line is the sum of the two contributions. A low-rapidity source, inter-

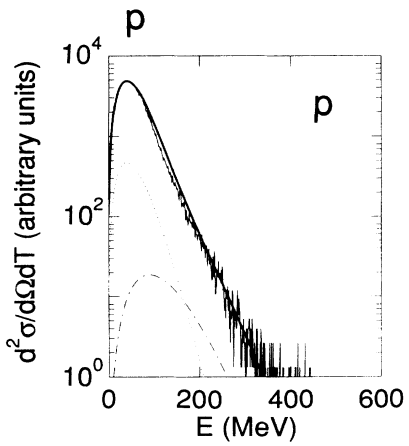

FIG. 9. This figure shows an example of the fitting procedure used to extract the spectral slope parameter for protons at zero degrees. The dotted line is the intermediate-rapidity source component used to fit the peak of the distribution with a source velocity equal to one-half the beam velocity. This curve is divided by 10 for clarity. The dot-dashed line is the component used to fit the tail with a source velocity equal to the beam velocity. This curve is divided by 10 for clarity. The solid double line is the sum of the two components.

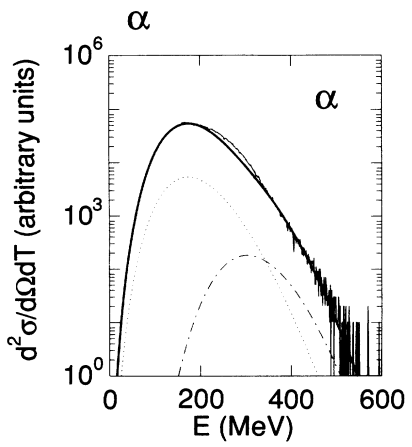

FIG. 10. This figure shows an example of the fitting of a 0° α spectrum. The conditions of Fig. 9 apply.

preted as an evaporative target contribution [11], was not used since the measurements were not extended to extreme back angles.

The angular distributions of the six-particle types are shown in Figs. 11–16. The individual points were determined by averaging over a 7-MeV bin centered at the indicated energy. The energy is indicated to the right and above the curve. The energy curves have a 50-MeV difference between successive curves. The solid lines are only to guide the eye. Curves which have only one point, at 0°, should be considered upper limits to the cross sections.

In general, these distributions show the cross sections being highly peaked in the forward direction, that is, forward of 20° in the laboratory and the cross sections then decreasing more slowly at the back angles. This would indicate a two-component source; the first source being a high-velocity source which is responsible for the formation of high-energy particles at forward angles; the second source being a lower-velocity source which is responsible for the low-energy particles, which are emitted more nearly isotropically. The first source may represent a hot-spot source [46–50] in which a small region of the colliding nuclei is locally heated to relatively large temperatures—that is, temperatures greater than the LI binding energies—this region is in a preequilibrium state and can cool by the emission of one or more energetic light particles. This mechanism is somewhat analogous to pionic fusion in which an excited nucleus, or region within a nucleus, cools by the emission of pions. The second source is similar to a compound-nuclear source, in which case the nuclei are either in thermal equilibrium or well along the kinetic path to equilibrium. Such a source would be nearly isotropic in the frame of reference of the

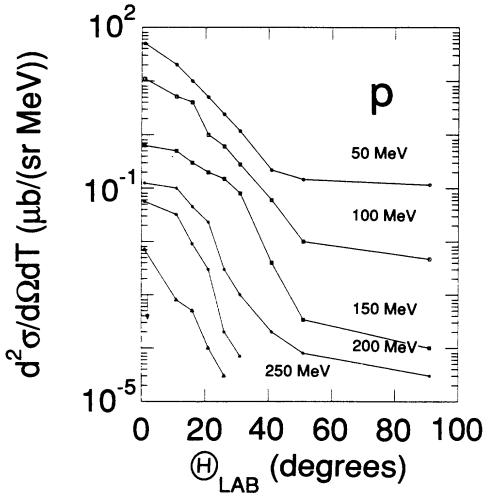

FIG. 11. The angular distribution of fragmentation cross sections for protons from 50 to 350 MeV. The individual points were determined by averaging over a 7-MeV bin centered at the indicated energy. The 0° point at 350 MeV is an upper limit. The solid lines are to guide the eye only.

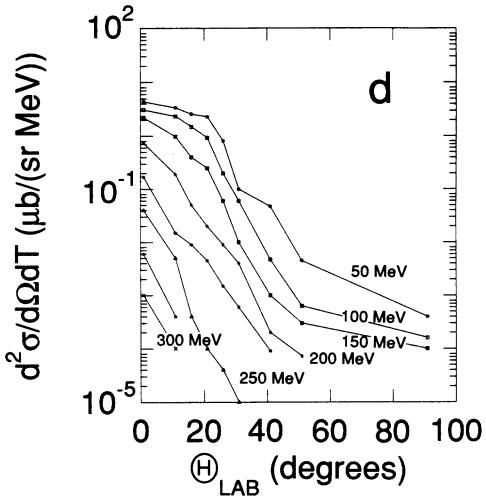

FIG. 12. The angular distribution of fragmentation cross sections for deuterons from 50 to 400 MeV. The conditions of Fig. 11 apply.

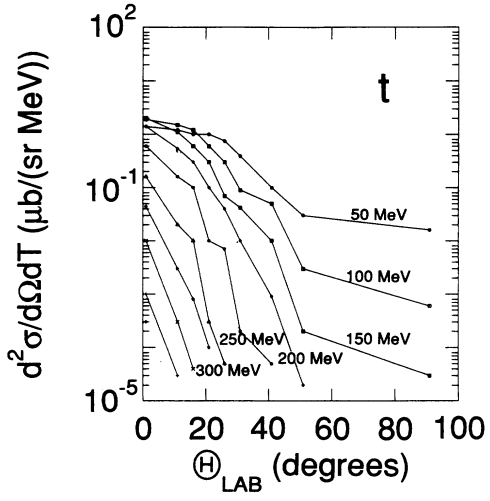

FIG. 13. The angular distribution of fragmentation cross sections for tritons from 50 to 500 meV. The 0° point as 500 MeV is an upper limit. The conditions of Fig. 11 apply.

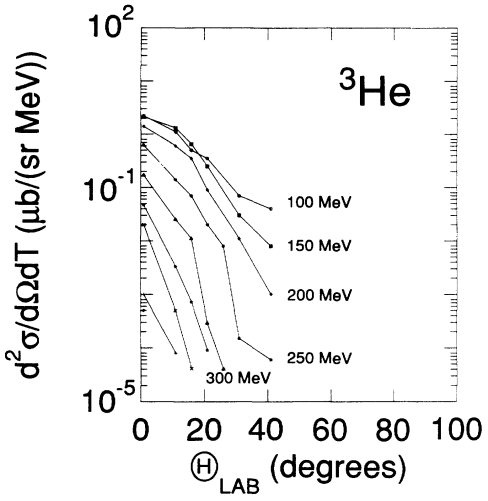

FIG. 14. The angular distribution of fragmentation cross sections for ^{3}He from 100 to 500 MeV. The 0° point at 500 MeV is an upper limit. The conditions of Fig. 11 apply.

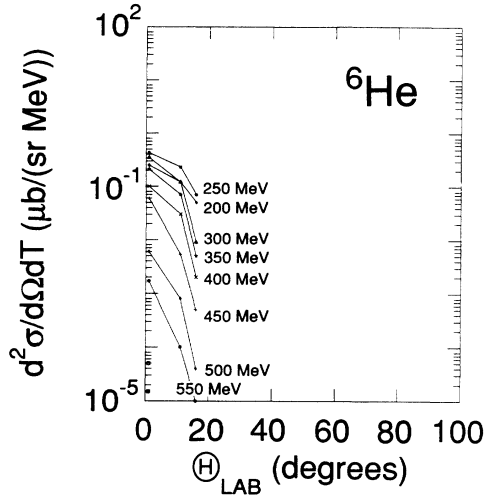

FIG. 16. The angular distribution of fragmentation cross sections for ^{6}He from 250 to 600 MeV. The 0° point at 600 MeV is an upper limit. The conditions of Fig. 11 apply.

source nuclei, and so more nearly isotropic in the laboratory frame. The source temperatures of such a CN system would be equal to, or slightly higher than, the typical Fermi energy of a compound nucleis, i.e., a few MeV. The emission from such a CN system would be a nearly thermal evaporation process.

Examples of moving-source model fits to the angular distributions are shown in Figs. 17 and 18 for 200-MeV proton and alpha particles, respectively. The dashed lines show the contribution from the high-rapidity source, with an apparent source temperature of 13±1 MeV for the protons, and 8.3±0.7 MeV for the alphas. The dot-dashed lines represent the intermediate-rapidity source with temperatures of 8.6±0.7 for the protons, and 11±0.9 MeV for the alphas. The temperatures were determined by a least-squares fit by the moving-source model, the quoted errors are the errors determined from the error matrix in the fitting routine only, and do not include any estimates of systematic errors. The contributions from the two sources are divided by a factor of 10 for clarity. The dotted lines are the sum of the two contributions, while the solid lines connect the data points and are only to guide the eye.

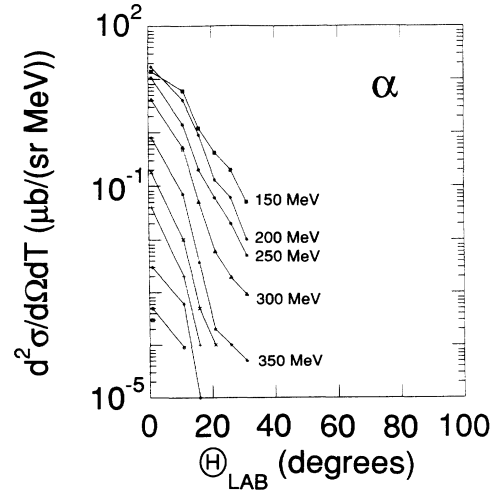

FIG. 15. The angular distribution of fragmentation cross sections for α from 150 to 550 MeV. The 0° point at 550 MeV is an upper limit. The conditions of Fig. 11 apply.

C. Detector-hit multiplicities and particle yields

Coincidence events were also recorded on-line to event mode tapes and then analyzed off line. In addition to the three-particle telescopes described above, there was also a smaller BGO detector at −15°. While this fourth detector had no PID, it was possible to put a lower-energy

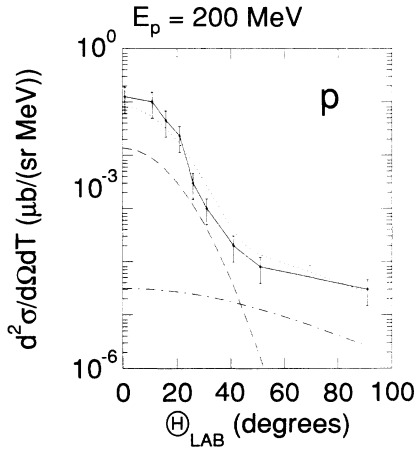

FIG. 17. This figure shows the fitting used to extract the spectral parameters for protons at 200 MeV. The dashed line shows the contribution from the high-rapidity source, with a source temperature of 13.3±1.0 MeV. The dot-dashed line represents the intermediate-rapidity source with temperatures of 8.6±0.7 MeV. The contribution for these two sources is divided by a factor of 10 for clarity. The dotted line is the sum of the two sources. The solid line is only to guide the eye.

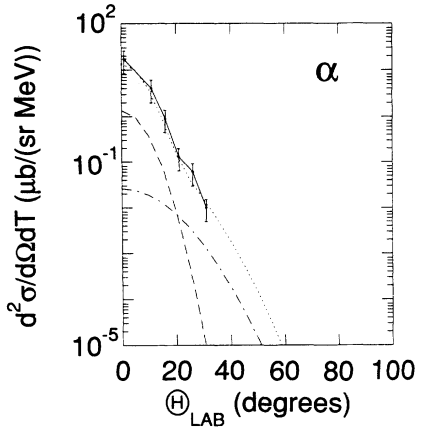

FIG. 18. This figure shows the fitting used to extract the spectral parameters for α at 200 MeV. The dashed line show the contribution from the high-rapidity source, with a source temperature of 8.3±0.7 MeV. The dot-dashed lines represent the intermediate-rapidity source with temperatures of 10.6±0.9 MeV. The contribution for these two sources is divided by a factor of 10 for clarity. The dotted line is the sum of the two cases. The solid line is only to guide the eye.

threshold on the detector. Thus, all four detectors could be set to find inclusive coincidences with LI particles—that is, the coincidence particles could be energetic light ions, heavy ions, or even γ rays, pions or electrons, but not neutrons since the BGO detectors have no significant neutron detection efficiency. The only requirement was that the energy measured in any of the coincidence BGO detectors had to be greater than 50 MeV and at least one of the particles had to be identified as a LI. The detector-hit multiplicities are shown in Fig. 19 and will be discussed below.

The forward-angle yields for particles at, or above, 40 MeV/nucleon are shown in Fig. 20. From this figure a trend can be noted for all the LI, except alphas, the yield drops with mass. There seems to be little, if any, correlation with charge, since the tritons and the ^{3}He have nearly identical yields. Not included in this graph are ^{8}He which had a total yield of less than 10^4 counts above 320 MeV (40 MeV/nucleon).

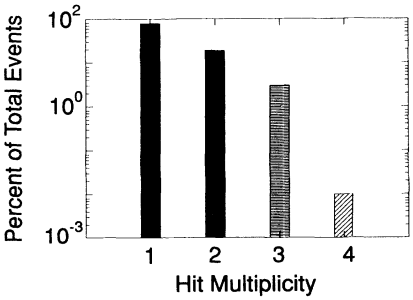

FIG. 19. The inclusive LI and γ-ray detector-hit multiplicity is shown in this figure. All events identified with a charge less than 3 and depositing more than 50 MeV total energy in each detector were included in this hit multiplicity spectrum.

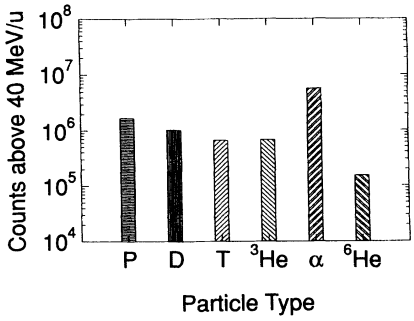

FIG. 20. The total yields of particles with energies greater than 40 MeV/nucleon for the entire experiment. Less than 10^4 ^{8}He were observed with E/A greater 40 MeV.

III. MOVING-SOURCE ANALYSIS

A. Thick target yields

The moving-source model is quite simple: one assumes that a source is moving with a velocity v_s and that the constituents, nucleons, within the source have a Maxwellian velocity distribution characterized by some source temperature T_s. The constraint upon the constituents is removed, the source "evaporates," and the constituents move out isotropically in the reference frame of the original moving source. As noted above, although these temperatures, T_s, are not nuclear equilibrium temperatures, the model is useful in comparing the results of various experiments which have used the same model, and can be used as a predictive tool to calculate projectile fragmentation yields.

To calculate the energy spectrum in the laboratory frame, one must boost the energy from the source frame to the laboratory frame, and multiply by the Jacobian. In the laboratory reference frame the doubly differential cross section for a particle of mass m may then be written [14,43] as

$$\frac{d^2\sigma}{d\Omega\, dE} = N_0 \sqrt{E_R} \exp^{(-E_R/T_s)} . \tag{1}$$

The laboratory doubly differential cross sections can be calculated in the normal manner from the laboratory yields.

As discussed in previous papers [14,51], the thick target yield in the laboratory may be written as the integral of a thin target yield divided by the energy loss integrated over the range of the particle in the target

$$\frac{dN}{dE_{\rm lab}} = \int_0^{E^0_{\rm max}} \frac{dN_0/dE_{\rm lab}}{dE_{\rm lab}/dx} dE_{\rm lab}$$
$$= N_0 E^{\beta}_{\rm lab} e^{-E_{\rm lab}/T_{\rm lab}} , \tag{2}$$

where $\frac{1}{2} \le \beta \le 1$. As noted in these previous papers, the value of the parameter β approaches the limit of $\frac{1}{2}$ as the laboratory energy increases. We note that this expression is only valid for the high-energy portion of the energy spectrum, since we have only considered the high-velocity component of the velocity distribution of the

original source, as can be seen in Eq. (1). However, one can use the high-energy portion of laboratory yields, via a fitting procedure with Eq. (2), to find values of the source temperature and velocity from stopped target measurements at 0°.

B. Fits to the data

For each particle type observed, at each angle of observation, the laboratory yield was fit by Eq. (2) using a least-squares method. In the fit the normalization constant, N_0, and the source temperature, T_s, were free parameters while the source velocity was set to various values. For forward angles, $0° \leq \theta_{\text{lab}} \leq 20°$, separate fits were made for fixed values of v_s, these data will be referred to as the small-angle data. The values of v_s used were $v_s = v_{\text{beam}}$, $v_s = 0.9 v_{\text{beam}}$, and $v_s = 0.8 v_{\text{beam}}$. For laboratory angles greater than 20°, referred to as the large-angle data, the fixed values of v_s used in the fit were $v_s = 0.7 v_{\text{beam}}$, $v_s = 0.6 v_{\text{beam}}$, $v_s = 0.5 v_{\text{beam}}$, and $v_s = 0.4_{\text{beam}}$.

The values of v_s used in the fits of the laboratory yields correspond to previously reported results of heavy-ion (HI) collisions [2–14,16,17]. The large-angle data are characterized by individual, incoherent nucleon-nucleon collisions [2–13] in which the source velocity is thus equal to about half the beam velocity and the source temperature is very near the conventional Fermi temperatures of about 5 MeV. In this mechanism the projectile nucleus is not significantly excited, since collisions are between individual nucleons, thus the nuclear emission temperature is not increased.

In contrast, the small-angle data are not well described by nucleon-nucleon collisions [8–13,14,16,17,40] but rather need source velocities approximately equal to the beam velocities, and source temperatures significantly larger than normal nuclear equilibrium temperatures [52,53]. The model often used for the small-angle data is then that of a projectile being excited locally by passage near a target nucleus, increasing the projectile temperature, and then fragmenting. The target nucleus is assumed to be a spectator in this process. This model leads to two distinct features in the predicted energy spectrum: first, there is a peak in the spectrum near $(E/A)_{\text{spec}} = (E/A)_{\text{beam}}$ with a width that is related to typical equilibrium nuclear temperatures [54,55]. Secondly, there is the previously discussed high-energy tail in the energy spectrum which is characterized by a temperature greater than normal nuclear Fermi temperatures. The two features of this model may be explained as follows: a small region of the projectile nucleus becomes highly excited, such a region is called a hot spot, this region is not in thermal equilibrium with the remainder of the nucleus; the rest of the nucleus either is not excited or is only slightly excited. Fragmentation occurs in the projectile nucleus, without the hot spot and the remainder of the nucleus achieving thermal equilibrium. The nucleons that were in the hot spot are characterized by a temperature greater than the Fermi temperature of the parent nucleus, while the nucleons in the remaining portion of the projectile nucleus are still characterized by the initial nuclear temperature. Any emitted particles originating from the "cool" portion of the projectile nucleus would have been produced by a quasifree process, while nucleons or other LI originating from the hot spot would be from a deep-inelastic source [46,50]. The important part of the model is that the fragmentation occurs so quickly that the projectile nucleus is unable to achieve thermal equilibirum, and the particles emitted are then characteristic of two different source populations.

The angular distributions in Figs. 17 and 18 show calculations using the moving-source model with source velocities approximately equal to the beam velocity and half the beam velocity is indicated on the figures. As expected, for $Z=1$ isotopes, the small-angle data are better represented by the high-velocity component, while the large-angle data seem to be represented by the low-velocity distribution. While for the $Z=2$ isotopes, the angular distributions can almost completely be described by the high-velocity component.

C. Discussion of apparent source temperatures

Tables II and III show source temperatures deduced from least-squares fits to the moving-source model to the high-energy portion of the laboratory yields. The laboratory temperatures are the values returned from the least-squares analysis of the high-energy portions of the spectra, with the errors being the sum of the probable errors returned from the fitting routine, the estimate of errors due to the resolution of the BGO crystals, and an esti-

TABLE II. Summary of results.

Angle (deg)	v_s/v_{beam} used in fit	Protons T_{lab} (MeV)	Protons T_{source} (MeV)	Deuterons T_{lab} (MeV)	Deuterons T_{source} (MeV)	Tritons T_{lab} (MeV)	Tritons T_{source} (MeV)
0	0.9	33±4.1	17±2.0	29±3.1	10±1	31±3.5	7±1.0
10	0.9	21±2.0	10±1.8	20±2.0	9±1.2	27±3.0	7±1.0
15	0.9	16±1.5	8±1.4	19±2.1	8±1.1	25±2.5	6±1.7
20	0.5	17±1.7	6±1.3	20±2.0	12±1.8	27±2.8	13±1.5
25	0.5	17±1.7	12±1.8	19±2.0	11±1.6	22±3.0	12±1.8
30	0.5	17±1.7	11±1.1	17±2.1	10±1.4	29±2.6	11±1.6
40	0.5	15±1.5	8±1.0	22±2.3	7±1.0	22±2.3	8±1.4
50	0.5	14±1.5	8±0.8	20±2.1	7±1.1	21±2.0	6±1.2
90	0.5	14±1.2	7±0.7	14±1.7	5±1.2	12±1.4	4±0.7

TABLE III. Summary of results.

Angle (deg)	v_s/v_{beam} used in fit	^{3}He T_{lab} (MeV)	^{3}He T_{source} (MeV)	^{4}He T_{lab} (MeV)	^{4}He T_{source} (MeV)	^{6}He T_{lab} (MeV)	^{6}He T_{source} (MeV)
0	0.9	32±3.5	9±1.5	31±3.9	8±1.2	34±4.1	8±1.4
10	0.9	26±2.9	8±1.5	23±2.5	7±1.0	36±4.2	11±1.6
15	0.9	23±2.5	7±1.4	26±3.2	9±1.3	36±4.4	7±1.1
20	0.5	23±2.5	14±1.6	29±3.6	13±1.9		
25	0.5	22±2.4	14±1.8	27±3.4	13±1.8		
30	0.5			24±2.6	10±1.4		

mate of the errors due to nuclear reactions within the BGO crystal, where all errors have been added in quadrature. The errors in the source temperature reflect the probable errors returned from the fitting routine and differences in source temperature when the source velocity is changed by ±10%, as well as the systematic errors mentioned above. Again the errors are added in quadrature. The source velocity used in the fitting routine was $v_s=0.9v_{beam}$ for angles less than 20° and $v_s=0.5v_{beam}$ for angles equal to or greater than 20°.

These values of v_s are chosen to be equal to values used in the analysis of our previous experiments [14], so that a direct and consistent comparison of the results may be made of the extracted parameters. The values calculated using $v_s=v_{beam}$ vary from the values reported here by less than 5%, which is, in general, less than the reported uncertainties.

We note first that the temperatures deduced at 0° are generally greater than conventional nuclear Fermi temperatures, with the one possible exception being the triton data. We also note that the deduced temperatures decrease with increasing mass number. The values for the temperatures deduced for ^{3}H and ^{3}He are equal within the estimated errors of each other, suggesting that the temperatures are essentially unaffected by either initial- or final-state interactions of the system. The $\theta=0°$ temperatures deduced from these measurements are very similar to temperatures we have reported previously [14] for protons and deuterons at a lower bombarding energy, while the deduced source temperatures for the alpha particles are slightly lower than previously reported. This suggests that the temperatures have become saturated, since this experiment was conducted with a projectile with nearly three times the energy per nucleon as our previously reported experiment, and yet the deduced source temperatures have not significantly increased. However, most of these temperatures are above the limiting equilibrium value of $\approx$8 MeV, the mean nucleon binding energy [56–58], that would be expected, independent of beam energy, if the beam energy was thermalized prior to fragmentation. Thus, the high temperatures near $\theta=0°$ are indicative of nonequilibrium processes, as also reported in previous experiments [59–61].

As discussed earlier, a saturation effect could be explained by a partitioning of the available energy among a number of emitted particles. If the available beam energy is relatively low, only one particle may obtain enough energy to be removed from the nucleus, with the rest of the energy being dissipated as internal excitation. An increase in beam energy may give more than one particle sufficient energy to be moved from the nucleus. This is analogous to a fluid boiling, increasing the energy supplied to the fluid does not increase the temperature of the fluid but rather causes an increase in the rate of vaporization. An experimental signature for a phase change is an abrupt change in the inferred lifetime, as deduced from proton correlations [30]. The inferred lifetimes would be long, $\sim 10^3$ fm/c, for evaporative emission from a liquid; the inferred lifetimes for an expanding and dispersing gas should be relative short, on the order of 100 fm/c.

For the $Z=1$ isotope group, the source temperatures deduced from the data are very similar to typical nuclear temperatures for angles greater than 40°, which is in agreement with previous measurements. On the other hand, the $Z=2$ isotope group has no appreciable yield above 150 MeV, the discriminator threshold, for these larger angles and hence there are no deduced temperatures in this region in our measurements.

IV. LIGHT-ION MULTIPLICITIES

The inclusive light-ion detector hit multiplicities for light ions and γ rays with an energy greater than 50 MeV, as discussed above, are shown in Fig. 19. These detector-hit multiplicities are related to the charged-particle multiplicities. Not included in this measurement, unfortunately, are the neutron events. Neutrons are a major source of emitted particles in these HI collisions, and form a large part of the particle multiplicity in such spectra [59]. Comparison of the multiplicities measured in this experiment to multiplicities measured in our previous experiment [14] show a marked increase in detector hits, an increase which cannot be explained by the modest increase in detector efficiency of this experiment. Again, the large LI multiplicities, and the marked increase of multiplicities with beam energy, supports the theory that most of the produced particle spectra, at small angles, are the result of projectile fragmentation with the emission of single or multiple particles [45], while the larger-angle particle spectra are mostly due to compound-nucleus evaporation, where the compound nucleus has sufficient time to reach thermal equilibrium before emission. This experiment did not measure the very large back angles where one would expect to see target-like-fragments (TLF's) dominating the spectra. But other experiments, particularly the neutron data of Wada *et al.* [11], shows data which is strongly dominated by TLF's at back angles.

V. DISCUSSION

The results of this experiment show two major features. First, the apparent source temperatures have only modestly increased, or remain relatively constant for the $Z=1$ isotopes, despite the fact that the energy of the beam, measured in energy per nucleon, is two to eight times greater than those used in our previous measurements [14]. For the α particles, the only $Z=2$ isotope for which we have previous data, the source temperature has actually decreased by what may be a statistically significant amount—that is, nearly two sigma—from the deduced alpha temperatures for 40 MeV/nucleon ^{16}O on ^{181}Ta. Second, the detector-hit multiplicity measurements indicate that the LI particle multiplicity has increased markedly going from an energy per nucleon of 30 MeV to an energy per nucleon of 85 MeV.

Associated with the first factor, the modest increase of source temperatures, is the corresponding lack of significant LI production near the full beam energy. In our previous measurements, with projectiles of atomic weight less than 32 at lower beam energies [14], LI particle production—particularly alpha particles—whose energy spectra stretched to nearly the full beam energy were observed. In comparison, the energy spectra of the alpha particles measured in this experiment only reached about one-third of the full beam energy. This indicates that the proposed mechanism of massive cluster transfers [16,17] is not significant at this energy. This may not be unexpected as the grazing angle for this energy has moved very nearly into 0° and all one-step direct transfer reactions are reduced. Whatever the cause, it seems clear that any coherent effects are greatly reduced at this bombarding energy, as one might expect for reactions far above the barrier energy.

ACKNOWLEDGMENTS

We thank the staff at the MSU-NSCL for their support during this experiment. We also thank Dave Hotz and Karim Ashktorab for their assistance on this experiment. This work was supported in part by NSF Grant Nos. PHY-8911831 (U.M.) and PHY-8911692 (U.M.D.), INT-8816221 (U.S.-China Cooperative Science Program). The MSU-NSCL is funded by the National Science Foundation.

[1] H.C. Britt and A. R. Quinton, Phys. Rev. **124**, 877 (1961).
[2] C. K. Gelbke, D. K. Scott, M. Bini, D. L. Hendrie, J. L. Laville, J. Mahoney, M. C. Mermaz, and C. Olmer, Phys. Lett. **70B**, 415 (1977).
[3] T. C. Awes, G. Poggi, C. K. Gelbke, B. B. Black, B. G. Giagola, H. Breuer, and V. E. Viola, Jr., Phys. Rev. C **24**, 89 (1981).
[4] C. B. Chitwood, D. J. Fields, C. K. Gelbke, D. R. Klesh, W. G. Lynch, M. B. Tsang, T. C. Awes, R. L. Ferguson, F. E. Obenshain, F. Plasil, R. L. Robinson, and G. R. Young, Phys. Rev. C **34**, 858 (1986).
[5] R. L. Auble, J. B. Ball, F. E. Bertrand, R. L. Ferguson, C. B. Fulmer, I. Y. Lee, R. L. Robinson, G. R. Young, and J. R. Wu, Phys. Rev. C **25**, 2504 (1982).
[6] R. L. Auble, J. B. Ball, F. E. Bertrand, C. B. Fulmer, D. C. Hensley, I. Y. Lee, R. L. Robinson, P. H. Stelson, D. L. Hendrie, H. D. Holmgren, J. D. Silk, and H. Breuer, Phys. Rev. Lett. **49**, 441 (1982); R. L. Auble, J. B. Ball, F. E. Bertrand, C. B. Fulmer, D. C. Hensley, I. Y. Lee, R. L. Robinson, P. H. Stelson, C. Y. Wong, D. L. Hendrie, H. D. Holmgren, and J. D. Silk, Phys. Rev. C **28**, 1552 (1983).
[7] R. L. Auble, J. B. Ball, F. E. Bertand, R. L. Ferguson, I. Y. Lee, R. L. Robinson, and G. R. Young, Phys. Rev. C **37**, 390 (1988).
[8] M. N. Namboodiri, P. Gonthier, H. Ho, J. B. Natowitz, R. Eggers, L. Adler, P. Kasiraj, C. Cerruti, A. Chevarier, N. Chevarier, and A. Demeyer, Nucl. Phys. **A367**, 313 (1981).
[9] J. B. Natowitz, M. N. Namboodiri, L. Adler, R. P. Schmitt, R. L. Watson, S. Simon, M. Berlanger, and R. Choudhury, Phys. Rev. Lett. **47**, 1114 (1981).
[10] B. V. Jacak, G. D. Westfall, G. M. Crawley, D. Fox, C. K. Gelbke, L. H. Harwood, B. E. Hasselquist, W. G. Lynch, D. K. Scott, H. Stöcker, M. B. Tasng, G. Buchwald, and T. J. M. Symons, Phys. Rev. C **35**, 1751 (1987).
[11] R. Wada, D. Fabris, K. Hagel, G. Nebbia, Y. Lou, M. Gonin, J. B. Natowitz, R. Billerey, B. Cheynis, A. Demeyer, D. Drain, D. Guinet, C. Pastor, J. Alarja, A. Giorni, D. Heuer, C. Morand, B. Viano, C. Mazur, C. Ngo, S. Leray, R. Lucas, M. Ribrag, and E. Tomassi, Phys. Rev. C **39**, 497 (1989).
[12] H. R. Schelin, A. Galonsky, C. K. Gelbke, L. Heilbronn, W. G. Lynch, T. Murakami, M. B. Tsang, X. Yang, G. Zhang, B. A. Remington, F. Deak, A. Kiss, Z. Seres, and J. Kasagi, Phys. Rev. C **39**, 1827 (1989).
[13] M. Gonin, L. Cooke, K. Hagel, Y. Lou, J. B. Natowitz, R. P. Schmitt, B. Srivastava, W. Turmel, H. Utsunomiya, R. Wada, B. Fornal, G. Nardelli, G. Nebbia, G. Viesti, R. Zanon, G. Prete, P. Gonthier, and B. Wilkins, Phys. Lett. B **217**, 406 (1989).
[14] S. Shaheen, F. D. Becchetti, D. A. Roberts, J. W. Jänecke, and R. L. Stern, Phys. Rev. C **42**, 1519 (1990).
[15] D. E. Greiner, P. J. Lindstrom, H. H. Heckman, B. Cork, and F. S. Bieser, Phys. Rev. Lett. **28**, 926 (1976).
[16] C. Borcea, E. Gierlik, R. Kalpakakchieva, Yu. Ts. Oganessian, and Yu. E. Penionzhkevich, Nucl. Phys. **A351**, 312 (1981).
[17] H. Machner, D. Protic, G. Riepe, H. G. Bohlen, and H. Fuchs, Phys. Rev. C **31**, 443 (1985); H. Machner, in *Nuclear Physics Recent Trends and Developments*, edited by Z. Wilhelmi, G. Szeflinska, and M. Kicinska-Habior (Harwood, Chur, Switzerland, 1987), Vol. 10, p. 581.
[18] T. K. Murakami, W. Benenson, Y. Chen, J. Clayton, E. Kashy, J. Stevenson, C. L. Tam, K. Hanold, and M. Mohar, Phys. Rev. C **40**, 2079 (1989).
[19] Z. Majka, V. Abenante, Z. Li, N. G. Nicolis, D. G. Sarantites, T. M. Semkow, L. G. Sobotka, D. W. Stracener, J. R. Beene, D. C. Hensley, and H. C. Griffin, Phys. Rev. C **40**, 2124 (1989).
[20] Z. Chen, C. K. Gelbke, W. G. Gong, Y. D. Kim, W. G. Lynch, M. R. Maier, J. Pochodzalla, M. B. Tsang, F. Saint-Laurent, D. Ardouin, H. Delagrange, H. Doubre, J.

Kasagi, Al Kyanowski, A. Péghaire, J. Péter, E. Roasto, G. Bizard, F. Lefebvres, B. Tamain, J. Québerg and Y. P. Viyogi, Phys. Rev. C **36**, 2297 (1987).
[21] G. Röpke, Phys. Lett. **121B**, 223 (1983).
[22] R. A. Kryger, J. J. Kolata, W. Chung, S. Dixit, R. J. Tighe, J. J. Vega, P. A. DeYoung, C. Copi, J. Sarafa, D. G. Kovar, G. P. Golfoyle, and S. K. Sigworth, Phys. Rev. Lett. **65**, 2118 (1990).
[23] W. G. Gong, W. Bauer, C. K. Gelbke, N. Carlin, R. T. de Souza, Y. D. Kim, W. G. Lynch, T. Murakami, G. Poggi, D. P. Sanderson, M. B. Tsang, H. M. Xu, S. Pratt, D. E. Fields, K. Kwiatkowski, R. Planeta, V. E. Viola, Jr., and S. J. Yennello, Phys. Rev. Lett. **65**, 2114 (1990).
[24] S. E. Koonin, Phys. Lett. **70B**, 43 (1977).
[25] F. Zarbakhsh, A. L. Sagle, F. Brochard, T. A. Mulera, V. Perez-Mendez, R. Talaga, I. Tanihata, J. B. Carol, K. S. Ganezer, G. Igo, J. Oostens, D. Woodward, and R. Sutter, Phys. Rev. Lett. **46**, 1268 (1981).
[26] H. A. Gustafsson, H. H. Gutbrod, B. Kolb, H. Löhner, B. Ludewigt, A. M. Poskanzer, T. Renner, H. Reidesel, H. G. Ritter, A. Warwick, F. Weik, and H. Wieman, Phys. Rev. Lett. **53**, 544 (1984).
[27] W. G. Lynch, C. B. Chitwood, M. B. Tsang, D. J. Fields, D. R. Klesch, C. K. Gelbke, G. R. Young, T. C. Awes, R. L. Ferguson, F. E. Obenshain, F. Plasil, R. L. Robinson, and A. D. Panagiotou, Phys. Rev. Lett. **51**, 1850 (1983).
[28] Z. Chen, C. K. Gelbke, J. Pochodzalla, C. B. Chitwood, D. J. Fields, W. G. Lynch, and M. B. Tsang, Phys. Lett. B **186**, 280 (1987).
[29] J. Pochodzalla, C. B. Chitwood, D. J. Fields, C. K. Gelbke, W. G. Lynch, M. G. Tsang, D. H. Boal, and J. C. Shillcock, Phys. Lett. B **174**, 36 (1986).
[30] S. Pratt and M. B. Tsang, Phys. Rev. C **36**, 2390 (1987).
[31] T. C. Awes, R. L. Ferfuson, F. E. Obenshain, F. Plasil, G. R. Young, S. Pratt, Z. Chen, C. K. Gelbke, W. G. Lynch, J. Pochodzalla, and H. M. Xu, Phys. Rev. Lett. **61**, 2665 (1988).
[32] N. R. Dagdeviren, Phys. Lett. B **176**, 283 (1986).
[33] J. Pochodzalla, W. A. Friedman, C. K. Gelbke, W. G. Lynch, M. Maier, D. Ardouin, H. Delagrange, H. Doubre, C. Grégoire, A. Kyanowski, W. Mitting, A. Péghaire, J. Péter, F. Saint-Laurent, Y. P. Viyogi, B. Zwieglinski, G. Bizard, F. Lefebvres, B. Tamain, and J. Québert, Phys. Lett. **161B**, 275 (1985).
[34] C. B. Chitwood, C. K. Gelbke, J. Pochodzalla, Z. Chen, D. J. Fields, W. G. Lynch, R. Morse, M. B. Tsang, D. H. Boal, and J. C. Shillcock, Phys. Lett. B **172**, 27 (1986).
[35] J. Pochodzalla, C. K. Gelbke, W. G. Lynch, M. Maier, D. Ardouin, H. Delagrange, H. Doubre, C. Grégoire, A. Kyanowski, W. Mittig, A. Péghaire, J. Péter, F. Saint-Laurent, B. Zwieglinski, G. Bizard, F. Lefebvres, B. Tamain, J. Québert, Y. P. Viyogi, W. A. Friedman, and D. H. Boal, Phys. Rev. C **35**, 1695 (1987).
[36] Z. Chen, C. K. Gelbke, J. Pochodzalla, C. B. Chitwood, D. J. Fields, W. G. Gong, W. G. Lynch, and M. B. Tsang, Nucl. Phys. **A473**, 564 (1987).
[37] Z. Chen, C. K. Gelbke, W. G. Gong, Y. D. Kim, W. G. Lynch, M. R. Maier, J. Pochodzalla, M. B. Tsang, F. Saint-Laurent, D. Ardouin, H. Delagrange, H. Doubre, J. Kasagi, A. Kyanowski, A. Péghaire, P. Péter, E. Rosato, G. Bizard, F. Lefebvres, B. Tamain, J. Québert, and Y. P. Viyogi, Phys. Lett. B **199**, 171 (1987).
[38] F. Saint-Laurent, A. Kyanowski, D. Ardouin, H. Delagrange, H. Doubre, C. Grégoire, W. Mittig, A. Péghaire, J. Péter, G. Bizard, F. Lefebvres, B. Tamain, J. Québert, Y. P. Viyogi, J. Pochodzalla, C. K. Gelbke, W. Lynch, and M. Maier, Phys. Lett. B **202**, 190 (1988).
[39] H. M. Xu, W. G. Lynch, C. K. Gelbke, M. B. Tsang, D. J. Fields, M. R. Maier, D. J. Morrissey, T. K. Nayak, J. Pochodzalla, D. G. Sarantites, L. G. Sobotka, M. L. Halbert, and D. C. Hensley, Phys. Rev. C **40**, 186 (1989).
[40] F. D. Becchetti, P. M. Lister, and C. E. Thorn, Nucl. Instrum. Methods **225**, 280 (1984).
[41] S. Shaheen, F. D. Becchetti, D. Roberts, J. Jänecke, P. Schulman, R. Stern, A. Nadasen, and D. Kovar (unpublished).
[42] S. Shaheen, F. D. Becchetti, J. W. Jänecke, D. A. Roberts, and A. Nadasen, in Proceedings of the Fifth International Conference on Clustering Aspects in Nuclear and Subnuclear Systems, Kyoto, Japan, 1988 [Suppl. J. Phys. Soc. Jpn. **58**, 274 (1989)].
[43] S. Shaheen, Ph.D. thesis, University of Michigan, 1989.
[44] B. J. Fineman, D. H. Dowell, and A. M. Sandorfi, Brookhaven National Laboratory Report LEGS-8, 1983.
[45] J. Pouliot, Y. Chan, D. E. DiGregorio, B. A. Harmon, R. Knop, C. Moisan, R. Roy, and R. G. Stokstad, Phys. Rev. C **43**, 735 (1991).
[46] G. D. Westfall, J. Gossett, P. J. Johansen, A. M. Poskanzer, W. G. Meyer, H. H. Gutbrod, A. Sandavol, and R. Stock, Phys. Rev. C **37**, 1201 (1976).
[47] G. D. Westfall, B. V. Jacak, N. Anataraman, M. W. Curtin, G. M. Crawley, C. K. Gelbke, B. Hasselquist, W. G. Lynch, D. K. Scott, B. M. Tsang, M. J. Murphy, T. J. M. Symons, R. Legrain, and T. J. Majors, Phys. Lett. **116B**, 118 (1982).
[48] D. J. Fields, W. G. Lynch, C. B. Chitwood, C. K. Gelbke, M. B. Tsang, H. Utsunomiya, and J. Aichelin, Phys. Rev. C **30**, 1912 (1984).
[49] M. Prakash, P. Braun-Munzinger, and J. Stachel, Phys. Rev. C **33**, 937 (1986).
[50] J. Aichelin and G. Bertsch, Phys. Lett. **138B**, 350 (1984).
[51] T. Nakamwia, Nucl. Instrum. Methods A **240**, 207 (1985).
[52] L. Anderson, W. Brückner, E. Moeller, S. Nagamiya, S. Nissen-Meyer, L. Schroeder, G. Shapiro, and H. Steiner, Phys. Rev. C **28**, 1224 (1983).
[53] E. J. Moniz, I. Sick, R. R. Whitney, J. R. Ficenec, R. D. Kephart, and W. P. Trower, Phys. Rev. Lett. **26**, 445 (1971).
[54] H. Feshbach and K. Huang, Phys. Rev. **47B**, 300 (1973).
[55] A. S. Goldhaber, Phys. Lett. **53B**, 306 (1974); A. S. Goldhaber and H. H. Heckman, Annu. Rev. Nucl. Part. Sci. **28**, 161 (1978).
[56] C. Guet, Nucl. Phys. **A400**, 191 (1983).
[57] R. A. Dayras and G. Bizard, J. Phys. C **4**, 230 (1986).
[58] J. Bondorf, R. Donangelo, I. N. Mishustin, and H. Schulz, Nucl. Phys. **A444**, 460 (1985).
[59] D. Hilscher, Nucl. Phys. **A471**, 77 (1987).
[60] *Nuclear Dynamics and Nuclear Disassembly*, edited by J. B. Natowitz (World-Scientific, Singapore, 1989).
[61] H. Bohlen, A. Budzanowski, K. Grotowski, H. Homeyer, and T. Kozik, Hahn-Meitner Institute Annual Progress Report 449, 1987.

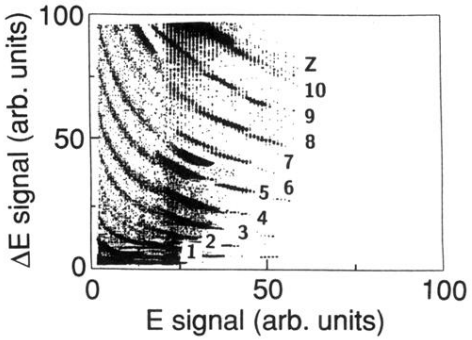

FIG. 1. This figure shows a particle identification spectrum which is the summation of several calibration runs. The vertical axis is the linear signal from the solid-state detector, the front element in the particle telescope. The horizontal axis is the light output from the last dynode of the photomultiplier which was attached to a BGO crystal, the last element in the particle telescope. This spectrum was taken with the amplifier from the solid-state detector set at a low gain; note that bands from $Z = 1$ (H) to $Z = 10$ (Ne) are visible.

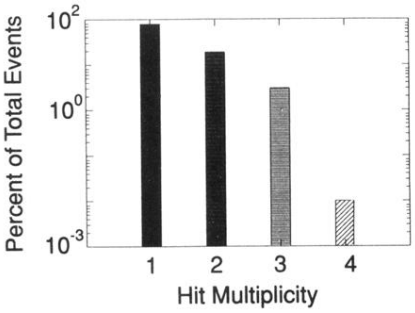

FIG. 19. The inclusive LI and γ-ray detector-hit multiplicity is shown in this figure. All events identified with a charge less than 3 and depositing more than 50 MeV total energy in each detector were included in this hit multiplicity spectrum.

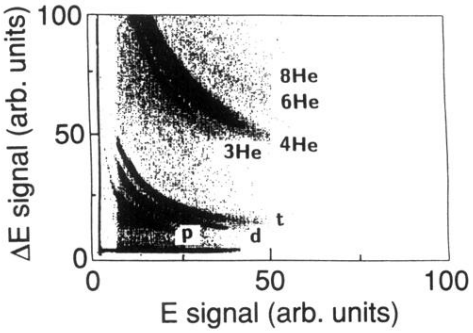

FIG. 2. This particle identification spectrum was taken with the amplifier from the solid-state detector set to a high-gain value and was used to identify the low-Z fragments. Note that all three isotopes of hydrogen are easily distinguished, p,d,t, and that three isotopes of helium are also clearly discernable (^{3}He,^{4}He,^{6}He). Evidence also exists in these spectra for the isotope ^{8}He.

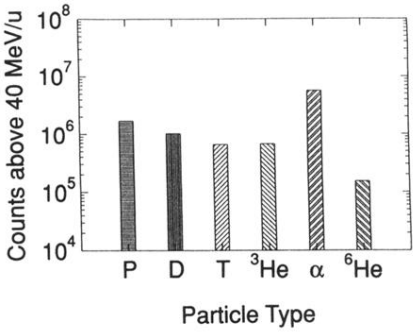

FIG. 20. The total yields of particles with energies greater than 40 MeV/nucleon for the entire experiment. Less than 10^4 ^{8}He were observed with E/A greater 40 MeV.